sciendo

Int. J. of Applied Mechanics and Engineering, 2020, vol.25, No.2, pp.157-175
DOI: 10.2478/ijame-2020-0027

MHD FREE CONVECTION-RADIATION INTERACTION IN A POROUS MEDIUM - PART II: SORET/DUFOUR EFFECTS

B. VASU
Department of Mathematics
Motilal Nehru National Institute of Technology Allahabad
Prayagraj- 211004, INDIA

Rama Subba Reddy GORLA*
Department of Mechanical Engineering
Cleveland State University
Ohio, 44115, USA

P.V.S.N. MURTHY
Department of Mathematics, Indian Institute of Technology
Kharagpur- 721 302, INDIA

V.R. PRASAD
Department of Mathematics
Madanapalle Institute of Technology and Science
Madanapalle-517325, INDIA

O.A. BÉG
Solid Mechanics, Spray Research Group, School of Computing
Science and Engineering, University of Salford, Newton Building
Manchester, M5 4WT, UK

S. SIDDIQA
Department of Mathematics
COMSATS Institute of Information Technology
Attock, PAKISTAN

This paper is focused on the study of two dimensional steady magnetohydrodynamics heat and mass transfer by laminar free convection from a radiative horizontal circular cylinder in a non-Darcy porous medium by taking into account of the Soret/Dufour effects. The boundary layer equations, which are parabolic in nature, are normalized into non-similar form and then solved numerically with the well-tested, efficient, implicit, stable Keller–Box finite-difference scheme. Numerical results are obtained for the velocity, temperature and concentration distributions, as well as the local skin friction, Nusselt number and Sherwood number for several values of the parameters, namely the buoyancy ratio parameter, Prandtl number, Forchheimer number, magnetohydrodynamic body force parameter, Soret and Dufour numbers. The dependency of the thermophysical properties has been discussed on the parameters and shown graphically. Increasing the Forchheimer inertial drag parameter reduces velocity but elevates temperature and concentration. Increasing the Soret number and simultaneously reducing the Dufour number greatly boosts the local heat transfer rate at the cylinder surface. A comparative study of the previously published and present results in a limiting sense is made and an excellent agreement is found between the results.

Key words: non-Darcy porous media transport, magnetic field, horizontal circular cylinder, Soret number, Dufour number.

* To whom correspondence should be addressed

1. Introduction

Transport phenomena in porous media are used in many branches of engineering and applied physics. These include foam flooding of gas-saturated petroleum reservoirs, perfusion in poroelastic myocardium tissue, drug delivery in the cerebral zone, heat transfer in the human skin system (Escobar and Civan [1], Ng *et al*. [2], Nicholson [3]), biporous heat pipe flows for high power electronic device cooling, porous media semiconductor heat sink design, forest fire dynamics, geothermal energy systems, oil recovery (Jinliang Wang Catton [4], Douglas *et al*. [5]), geological contamination simulation (Cheng and Yeh [6]), metallic foam modelling in materials processing (Laschet *et al*. [7]) and solar energy cells (Becker *et al.* [8]). The vast majority of models have considered isotropic, homogenous porous media, usually employing the Darcy law, which is valid for low velocity, viscous-dominated transport. However, porous media are generally heterogeneous and exhibit variable porosity. An early study of flow through variable porosity media was conducted by Roblee *et al*. [9] for the case of radial variation in chemical engineering systems. Much later, a seminal theoretical and experimental study was presented by Vafai [10] who studied the influence of variable porosity and also inertial forces (Forchheimer drag) on thermal convection flow in porous media, with the channeling effect being studied in detail. He elucidated the qualitative aspects of variable porosity in generating the channeling effect with an asymptotic analysis.

These studies have all assumed the fluid to be electrically non-conducting. Many industrial fluids have this property owing to the presence of ions in the fluid and will therefore respond to a magnetic field. Zueco *et al*. [11] used network simulation to investigate the hydromagnetic heat transfer of a micro-structural liquid material in a vertical pipe containing a Darcy-Forchheimer porous medium. Makinde *et al*. [12] analyzed, using MAPLE software, the hydromagnetic Darcian flow in a rotating annular porous regime. Damseh*et al.* [13] used a difference technique to study the magneto-hydrodynamic thermophoretic particle deposition in mixed convection through a porous medium adjacent to a non-isothermal wall. These studies did not consider the cylindrical geometry which arises frequently in for example the manufacture of conducting polymers, composites, liquids with metallic intrusions etc. An important study of natural convection boundary layers in Darcian porous media was presented by Minkowycz and Cheng [14], although they did not consider the magnetic case. Recently, Hamzeh *et al.* [15]investigated the effect of radiation on magnetohydrodynamic free convection boundary of a solid sphere with Newtonian heating. Recently, Kumari and Gorla [16] presented solutions for the MHD boundary layer flow past a wedge in a non-Newtonian nanofluid.

Both Darcian and Darcy-Forchheimer (inertial) models have been employed extensively in radiative-convection flows in porous media. Takhar *et al*. [17] used an implicit difference scheme and the Cogley-Vincenti-Giles non-graymodel to simulate the radiation-convection gas flow in a non-Darcy porousmediumwith viscous heating effects. Takhar *et al*. [18] employed a Runge-Kutta-Merson shooting quadrature and the Rosseland diffusion algebraic radiation model to analyze the mixed radiation-convection flow in a non-Darcy porous medium, showing that temperature gradients are boosted with radiative flux. Hossain and Pop [19] studied radiation effects on free convection over a flat plate embedded in a porous medium with high-porosity. Pal and Chatterjee [20] developed a numerical model and studied the MHD mixed convection with the combined action of Soret and Dufour effects on heat and mass transfer of a power-law fluid over an inclined plate in a porous medium in the presence of variable thermal conductivity, thermal radiation, chemical reaction and Ohmic dissipation and suction/injection.

In all the above studies Soret/Dufour effects have been neglected. Such effects are significant when density differences exist in the flow regime. Soret and Dufour effects are important for intermediate molecular weight gases in coupled heat and mass transfer in fluid binary systems, often encountered in chemical process engineering. Both free and forced convection boundary layer flows with Soret and Dufour effects have been addressed by Abreu *et al.* [21]. Recently, Bég *et al.* [22] used the local non-similarity method with a shooting procedure to analyze mixed convective heat and mass transfer from an inclined plate with Soret/Dufour effects with applications in solar energy collector systems. Bhargava *et al*. [23] also studied oscillating hydromagnetic heat and mass transfer with Soret and Dufour effects. Seddeek [24] studied thermo-diffusion and diffusion-thermo effects on mixed convection flow over an accelerating surface with a heat source with suction/blowing for the case of variable viscosity. El-Kabeir and Chamkha [25] focused on

the study of heat and mass transfer by mixed convection over a vertical slender cylinder in the presence of chemical reaction and thermal-diffusion and diffusion-thermo effects. Bhattacharyya *et al.* [26] presented a mathematical model for the Soret and Dufour effects on the convective heat and mass transfer in a stagnation-point flow of a viscous incompressible fluid towards a shrinking surface.

The objective of the present paper is to investigate the effects of Soret (thermo-diffusion) and Dufour (diffusion-thermal) on the hydromagnetic convective boundary layer on a horizontal permeable cylinder embedded in a non-Darcy porous regime where radiation is included by assuming Rosseland diffusion approximation. An implicit numerical solution is obtained to the transformed boundary layer equations.

2. Mathematical analysis

A steady, laminar, two-dimensional, viscous, incompressible, electrically-conducting, buoyancy-driven convection boundary layer heat and mass transfer from a horizontal permeable cylinder embedded in a non-Darcy saturated regime with radiation and Soret/Dufour effects is analyzed. A uniform magnetic field B_0, is applied in the radial direction, i.e. normal to the cylinder surface. Figure 1a shows the flow model and physical coordinate system.

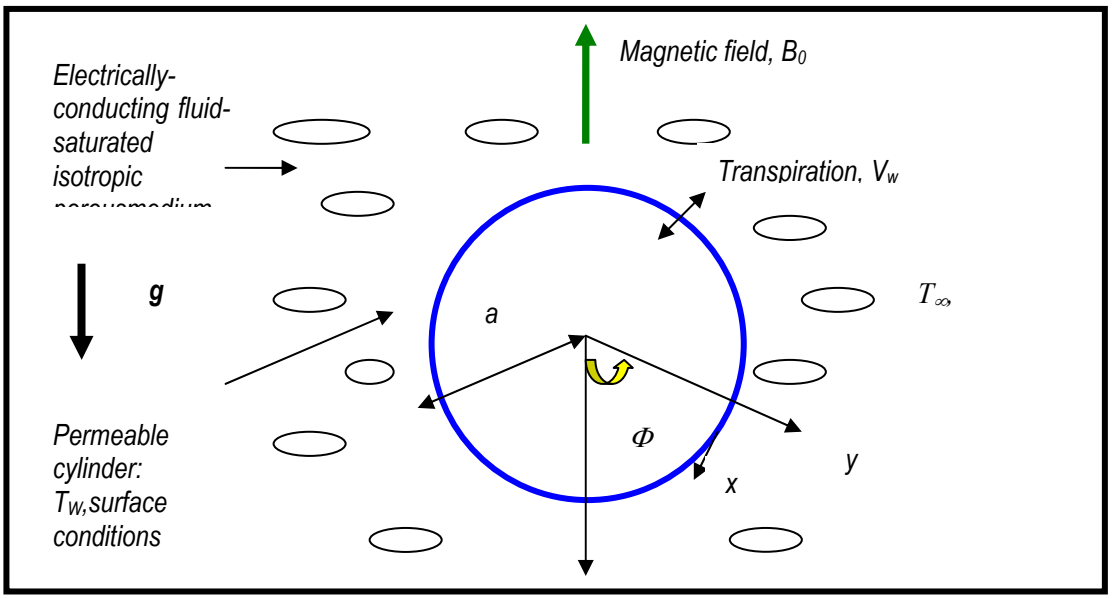

Fig.1a. Physical model and coordinate system.

The x-coordinate is measured along the circumference of the horizontal cylinder from the lowest point and the y-coordinate is measured normal to the surface, with '***a***' denoting the radius of the horizontal cylinder. $\Phi = x/a$, is the angle of the y-axis with respect to the vertical $(0 \le \Phi \le \pi)$. The gravitational acceleration g, acts downwards. The magnetic Reynolds number is assumed to be small enough to neglect magnetic induction effects. Hall current and ionslip effects are also neglected since the magnetic field is weak. We also assume that the Boussinesq approximation holds, i.e. that density variation is only experienced in the buoyancy term in the momentum equation. Additionally, the electron pressure (for weakly conducting fluids) and the thermoelectric pressure are negligible. Both the horizontal cylinder and the fluid are maintained initially at the same temperature and concentration. Instantaneously they are raised to a temperature T_w $(> T_\infty$, the ambient temperature of the fluid) and concentration C_w $(> C_\infty$, the far-field concentration) which remain unchanged. The fluid properties are assumed to be constant except the density variation in the buoyancy force term. In line with the approach of Yih [27] and introducing the boundary layer approximations, the governing conservation equations can be written as follows

$$\frac{\partial(u)}{\partial x}+\frac{\partial(v)}{\partial y}=0\,, \tag{2.1}$$

$$u\frac{\partial u}{\partial x}+v\frac{\partial u}{\partial y}=g\beta(T-T_\infty)\sin\left(\frac{x}{a}\right)+g\beta^*(C-C_\infty)\sin\left(\frac{x}{a}\right)+\nu\frac{\partial^2 u}{\partial y^2}-\frac{\sigma\beta_0^2}{\rho}u-\frac{\nu}{K}u-\Gamma u^2\,, \tag{2.2}$$

$$u\frac{\partial T}{\partial x}+v\frac{\partial T}{\partial y}=\alpha\frac{\partial^2 T}{\partial y^2}-\frac{1}{\rho c_p}\frac{\partial q_r}{\partial y}+\frac{D_m K_T}{c_s c_p}\frac{\partial^2 C}{\partial y^2}\,, \tag{2.3}$$

$$u\frac{\partial C}{\partial x}+v\frac{\partial C}{\partial y}=D_m\frac{\partial^2 C}{\partial y^2}+\frac{D_m K_T}{T_m}\frac{\partial^2 T}{\partial y^2}\,. \tag{2.4}$$

The boundary conditions are prescribed at the cylinder surface and the edge of the boundary layer regime, respectively, as follows

$$\begin{aligned} &u=0,\quad v=V_w,\quad T=T_w,\quad C=C_w \quad \text{at} \qquad y=0\,,\\ &u\to 0,\quad T\to T_\infty,\quad C\to C_\infty \quad \text{as} \quad y\to\infty \end{aligned} \tag{2.5}$$

where u and v are the velocity components in the x - and y - directions, respectively, K and Γ - the respective permeability and the inertia coefficient of the porous medium, ν is the kinematic viscosity of the conducting fluid, β and β^* - the coefficients of thermal expansion and concentration expansion, respectively, T and C - the temperature and concentration, respectively, σ - the electrical conductivity, B_0 - the externally imposed magnetic field in the y -direction, ρ - the density, D_m - the mass diffusivity, c_p - the specific heat capacity, c_s - the concentration susceptibility, α - the thermal diffusivity, T_m - the mean fluid temperature, K_T - the thermal diffusion ratio, T_∞ - the free stream temperature, C_∞ - the free stream concentration and V_w - the uniform blowing/suction velocity.

The Rosseland diffusion flux model is used and is defined following Modest [28] as follows

$$q_r=-\frac{4\sigma^*}{3k^*}\frac{\partial T^4}{\partial y} \tag{2.6}$$

where k^* is the mean absorption coefficient and σ^* is the Stefan-Boltzmann constant. Following Raptis and Perdikis [29] we can express the quadratic temperature function in Eq.(2.6) as a linear function of temperature. The Taylor series for T^4, discarding higher order terms can be shown to give

$$T^4\cong 4T_\infty^3-3T_\infty^4\,. \tag{2.7}$$

Substituting of this expression into Eq.(2.6) and then the heat conservation Eq.(2.3), eventually leads to the following form of the energy equation

$$u\frac{\partial T}{\partial x}+v\frac{\partial T}{\partial y}=\frac{1}{\rho c_p}\left(k+\frac{16\sigma^* T_\infty^3}{3k^*}\right)\frac{\partial^2 T}{\partial y^2}+\frac{D_m K_T}{c_s c_p}\frac{\partial^2 C}{\partial y^2}\,. \tag{2.8}$$

The stream function ψ is defined by $u=\partial\psi/\partial y$ and $v=-\partial\psi/\partial x$, and therefore, the continuity equation is automatically satisfied. In order to write the governing equations and the boundary conditions in dimensionless form, the following non-dimensional quantities are introduced.

$$\xi = \frac{x}{a}, \qquad \eta = \frac{y}{a}\sqrt[4]{\mathrm{Gr}}, \qquad f(\xi,\eta) = \frac{\psi}{\nu\xi\sqrt[4]{\mathrm{Gr}}},$$

$$\theta(\xi,\eta) = \frac{T-T_\infty}{T_w-T_\infty}, \qquad \phi(\xi,\eta) = \frac{C-C_\infty}{C_w-C_\infty}, \qquad \mathrm{Gr} = \frac{g\beta(T_w-T_\infty)a^3}{\nu^2},$$

$$\Lambda = \Gamma a, \qquad \mathrm{Da} = \frac{K\sqrt{\mathrm{Gr}}}{a^2}, \qquad N = \frac{\beta^*(C-C_\infty)}{\beta(T-T_\infty)}, \qquad F = \frac{kk_e}{4\sigma^* T_\infty^3}, \tag{2.9}$$

$$\mathrm{Pr} = \frac{\rho\nu c_p}{k}, \qquad \mathrm{Sc} = \frac{\nu}{D_m}, \qquad \mathrm{Du} = \frac{D_m K_T(C_w-C_\infty)}{c_s c_p \nu(T_w-T_\infty)},$$

$$\mathrm{Sr} = \frac{D_m K_T(T_w-T_\infty)}{\nu T_m(C_w-C_\infty)}, \qquad M = \sigma B_0^2 a^2 \big/ \rho\nu\sqrt{\mathrm{Gr}}, \qquad f_w = -V_w a \big/ \nu\sqrt[4]{\mathrm{Gr}}.$$

In view of Eq.(2.9), Eqs (2.1),(2.2),(2.8) and (2.4), reduce to the following coupled, nonlinear, dimensionless partial differential equations for momentum, energy and species conservation for the regime

$$f''' + ff'' - (1+\xi\Lambda)f'^2 + \frac{\sin\xi}{\xi}(\theta + N\phi) - \left(M + \frac{1}{Da}\right)f' = \xi\left(f'\frac{\partial f'}{\partial\xi} - f''\frac{\partial f}{\partial\xi}\right), \tag{2.10}$$

$$\frac{1}{\mathrm{Pr}}\left(1 + \frac{4}{3F}\right)\theta'' + f\theta' + \mathrm{Du}\phi'' = \xi\left(f'\frac{\partial\theta}{\partial\xi} - \theta'\frac{\partial f}{\partial\xi}\right), \tag{2.11}$$

$$\frac{\phi''}{\mathrm{Sc}} + f\phi' + \mathrm{Sr}\theta'' = \xi\left(f'\frac{\partial\phi}{\partial\xi} - \phi'\frac{\partial f}{\partial\xi}\right). \tag{2.12}$$

The transformed dimensionless boundary conditions are

$$\begin{aligned} &f' = 0, \quad f = f_w, \quad \theta = 1, \quad \phi = 1 \quad \text{at} \quad \eta = 0 \\ &f' \to 0, \quad \theta \to 0, \quad \phi \to 0 \quad \text{as} \quad \eta \to \infty \end{aligned} \tag{2.13}$$

where, the primes denote the differentiation with respect to η, the dimensionless radial coordinate, ξ is the dimensionless tangential coordinate and Φ the azimuthal coordinate, Λ - the local inertia coefficient (Forchheimer parameter), Da -the Darcy parameter, N - concentration to thermal buoyancy ratio parameter, k - thermal conductivity, Pr - the Prandtl number, Sc - the Schmidt number, Du - the Dufour number, Sr - the Soret number, M - the magnetic parameter, f_w - the blowing/suction parameter and Gr- the Grashof (free convection) parameter, F is the radiation parameter. $f_w<0$ for $V_w > 0$ (the case of blowing), and $f_w > 0$ for $V_w < 0$ (the case of suction). Of course, the special case of a solid cylinder surface corresponds to $f_W = 0$. The engineering design quantities of physical interest include the skin-friction coefficient, Nusselt number and Sherwood number, which are given by

$$\frac{1}{2}C_f\sqrt[4]{\mathrm{Gr}} = \xi f''(\xi,0), \tag{2.14a}$$

$$\frac{\mathrm{Nu}}{\sqrt[4]{\mathrm{Gr}}} = -\theta'(\xi,0)\,, \tag{2.14b}$$

$$\frac{\mathrm{Sh}}{\sqrt[4]{\mathrm{Gr}}} = -\phi'(\xi,0)\,. \tag{2.14c}$$

3. Results and discussion

The system of Eqs (2.10) – (2.12) subject to the boundary conditions (2.13) constitute a well-posed seven-first-order non-linear two-point boundary value problem. A numerical code developed and employed the efficient Keller-Box implicit finite difference method described by Cebeci and Bradshaw [30]. Further details of the solution procedure are documented in for example Rama Gorla and Vasu [31],and omitted here for conservation of space.

A representative set of numerical results is presented graphically to illustrate the influence of hydromagnetic parameter (M), Forchheimer inertial drag parameter (Λ),tangential coordinate (ξ), Dufour number (Du), Soret number (Sr), buoyancy ratio parameter (N) and radiation parameter (F) on velocity, temperature, concentration, shear stress, local Nusselt number and Sherwood number profiles. In all cases we have assumed the following default values (unless otherwise stated) for the parameters: Pr = *0.71* (air), Λ = *0.1* (weak second order Forchheimer drag), $F = 0.5$, $M = 1.0$ (equivalent hydromagnetic and viscous forces), Da= *0.1* (very high permeability of regime), $f_w = 0.5$. In order to verify the accuracy of our present method, we have compared our results with those of Merkin [32] and Yih [27]. Table 1 shows the comparisons of the values of $-\theta'(\xi,0)$.

Table 1. Values of the local heat transfer coefficient (Nu) for various values of ξ with $\mathrm{Da} \to \infty$, $\Lambda = 0$, $\mathrm{Pr} = 1$, $N = 0$, $f_w = 0$, $\mathrm{Sc} = 0$, $F \to \infty$, $\mathrm{Sr} = \mathrm{Du} = 0$.

ξ	$-\theta'(\xi,0)$		
	Merkin [32]	Yih [27]	Present results
0.0	*0.4212*	*0.4214*	*0.4214*
0.4	*0.4182*	*0.4184*	*0.4185*
0.8	*0.4093*	*0.4096*	*0.4097*
1.2	*0.3942*	*0.3950*	*0.3952*
1.6	*0.3727*	*0.3740*	*0.3741*
2.0	*0.3443*	*0.3457*	*0.3460*
2.4	*0.3073*	*0.3086*	*0.3087*
2.8	*0.2581*	*0.2595*	*0.2597*
π	*0.1963*	*0.1962*	*0.1964*

Figures 2a-b show the temperature and concentration distributions with collective variation in the Soret number (Sr) and Dufour number (Du). Sr represents the effect of temperature gradients on mass (species) diffusion. Du simulates the effect of concentration gradients on thermal energy flux in the flow domain. It is observed from Fig.2a that a decrease in Du from *5.0* through to *0.01* (simultaneously Sr increases from *0.01* to *5.0*, so that the product of Sr and Du remains constant i.e.,*0.05*) leads to a significant decrease in temperature values in the regime. Decreasing Du clearly reduces the influence of species gradients on the temperature field, so that θ values are clearly lowered and the boundary layer regime is cooled. From Fig.2b, it is noticed that ϕ (concentration function) in the boundary layer regime increases as Du decreases from *5.0* to *0.01* (and Sr simultaneously increases from *0.01* to *5.0*). Mass diffusion is evidently enhanced in the domain as a result of the contribution of temperature gradients. Unlike the temperature response (Fig.2a) a concentration overshoot accompanies the highest value of Sr, and arises in close proximity to the cylinder surface. In all other cases, the concentration profiles descend smoothly from a

maximum at the cylinder surface to the free stream. The influence of the Soret and Dufour terms will be relatively weak on the velocity fields, and these are therefore not plotted.

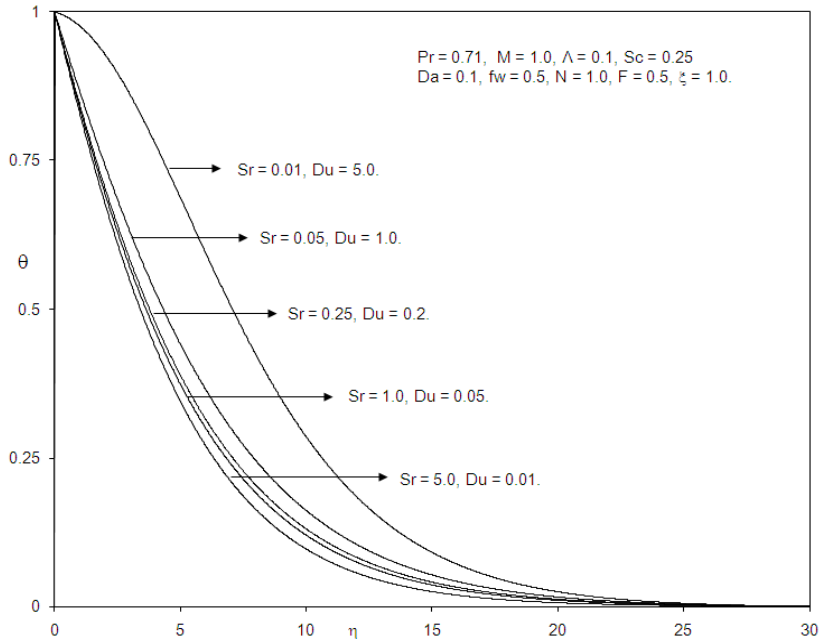

Fig.2a. Effect the Sr and Du on the temperature profiles.

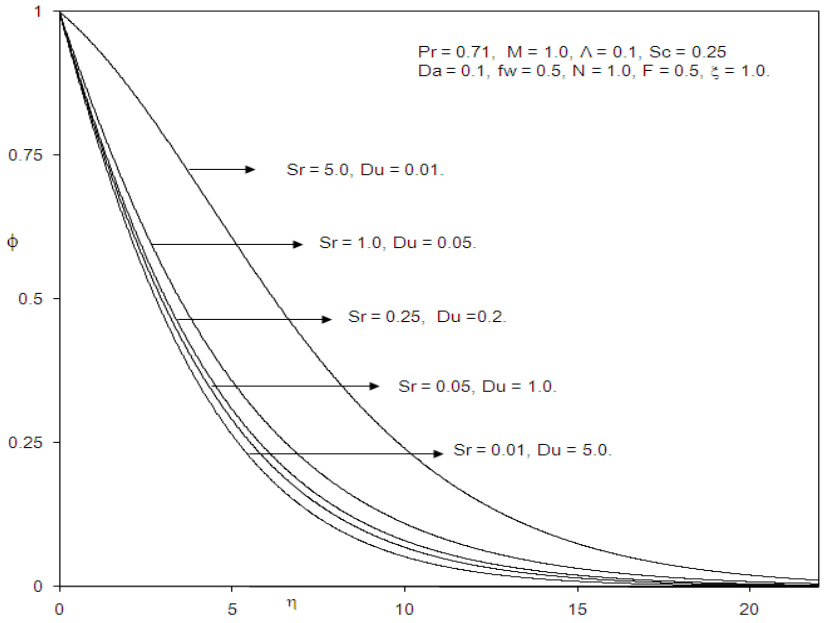

Fig.2b. Effect Sr and Du on the concentration profiles.

Figure 3 adepicts the velocity (f') response for different values of the Forchheimer inertial drag parameter (Λ), with radial coordinate (η). The Forchheimer drag force term, $\left(-\xi\Lambda f'^2\right)$ in the dimensionless momentum conservation Eq.(2.10) is quadratic and with an increase in Λ (which is infact related to the geometry of the porous medium) this drag force will increase correspondingly. As such the impedance offered by the fibers of the porous medium will increase and this will effectively decelerate the flow in the regime, as testified to by the evident decrease in velocities shown in Fig.3a. The Forchheimer effect serves to

superseed the Darcian body force effect at higher velocities, the latter is dominant for lower velocity regimes and is a linear body force. The former is dominated at lower velocities (the square of a low velocity yields an even lower velocity) but becomes increasingly dominant with increasing momentum in the flow, i.e. when inertial effects override the viscous effects (Fig.3a).

Figure 3b shows that temperature θ is increased continuously through the boundary layer with distance from the cylinder surface, with an increase in Λ, since with flow deceleration, heat will be diffused more effectively via thermal conduction and convection. The boundary layer regime will therefore be warmed with increasing Λ and boundary layer thickness will be correspondingly increased, compared with velocity boundary layer thickness, the latter being reduced.

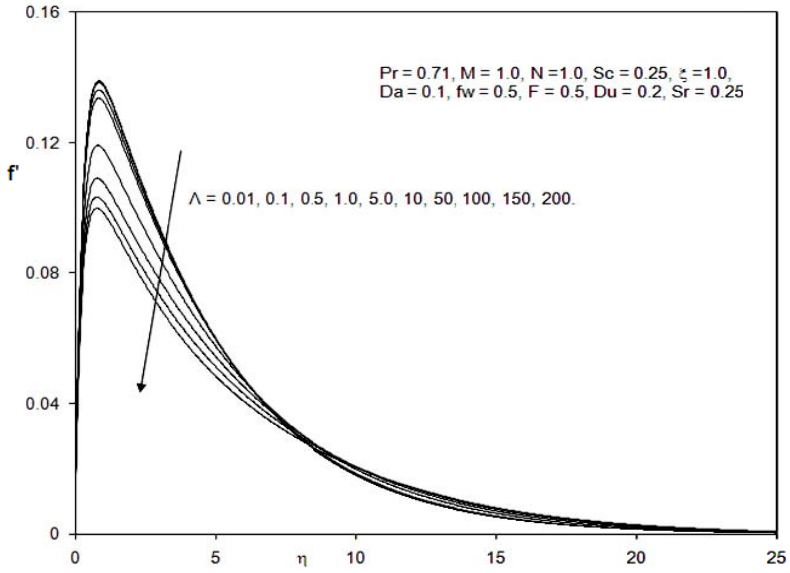

Fig.3a. Effect of Λ on the velocity profiles.

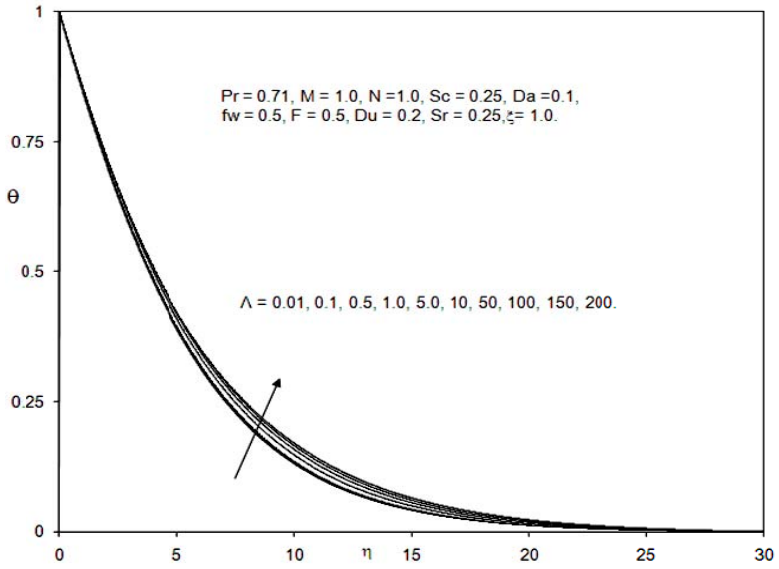

Fig.3b. Effect of Λ on the temperature profiles.

Figure 4a shows the influence of the magnetic parameter *M*, on the velocity field. An increase in *M*, strongly decelerates the flow. In all profiles a peak arises near the surface of the cylinder and this peak is displaced progressively closer to the wall with increasing *M* values. For *M = 1* the magnetic drag force will be of the same order of magnitude as the viscous hydrodynamic force. For *M > 1* hydromagnetic drag will

dominate and vice versa for $M < 1$. In magnetic materials processing, the flow can therefore be very effectively controlled with a magnetic field. Comparing with Fig.3a, it is observed that smaller increases in M have a more pronounced influence in decelerating the flow than very large changes in the Forchheimer parameter, despite the quadratic nature of the Forchheimer drag, indicating that the magnetic field has a greater effect on flow retardation than nonlinear porous drag. This is of immense importance in materials processing operations involving steady magnetic fields where even slight changes in field strength can be used to regulate flow.

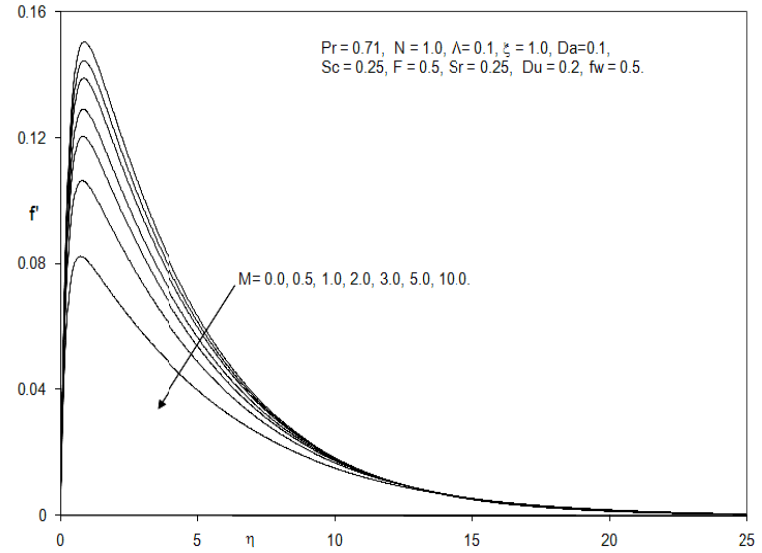

Fig.4a. Effect of M on the velocity profiles.

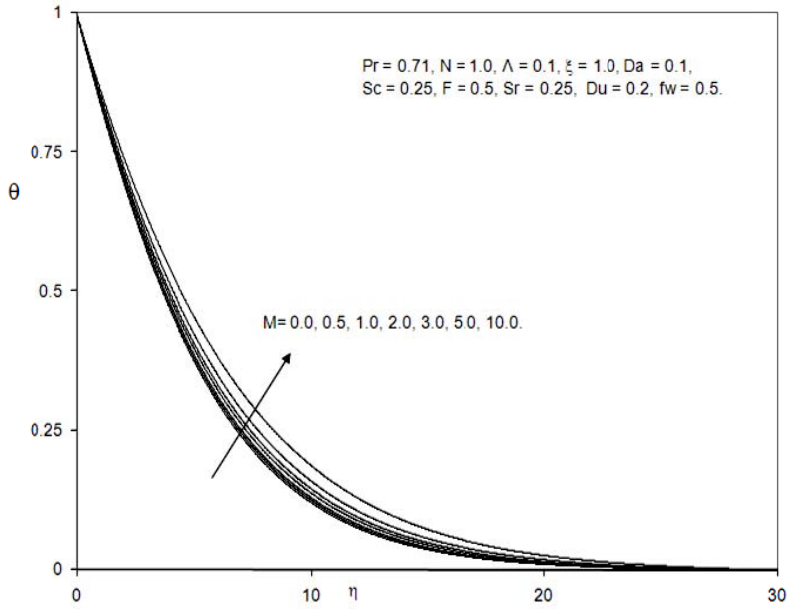

Fig.4b. Effect of M on the temperature profiles.

The temperature distribution in the boundary layer transverse to the cylinder surface is shown in Fig.4b for various values of the magnetic parameter. A marked increase in temperature is accompanied by a rise in M, i.e., temperatures are maximized with a strong magnetic field. The supplementary work expended in dragging the fluid in the boundary layer against the action of the Lorentzi an hydromagnetic drag is dissipated as thermal energy which heats the fluid. This induces a rise in temperatures.

Figures 5a-c illustrates the effect of the buoyancy ratio parameter, N, on velocity, temperature and concentration distributions through the boundary layer regime. For $N < 0$ velocity is strongly decelerated and the reverse effect is observed for $N > 0$, i.e. aiding buoyancy forces act to accelerate the flow, whereas opposing buoyancy forces effectively retard the flow. When $N=0$, the species buoyancy term vanishes and the momentum boundary layer Eq.(2.10) is a de-coupled the species diffusion (concentration) boundary layer Eq.(2.12). An increasing N from -0.5 to 5, clearly accelerates the flow, i.e., induces a strong escalation in stream wise velocity, f' close to the wall; thereafter velocities decay to zero in the free stream. Figure 5b indicates that with a rise in N, the temperature throughout the boundary layer is strongly reduced. Figure 5c shows that concentration ϕ exhibits the reduction to a positive increase in the buoyancy ratio, N; it is also reduced with increasingly negative values (opposing buoyancy forces). For all values of N there is a smooth decay inϕ profiles from a maximum at the cylinder surface to the free stream. The buoyancy effect can clearly be exploited to control concentration distributions in laminar flow from a cylinder.

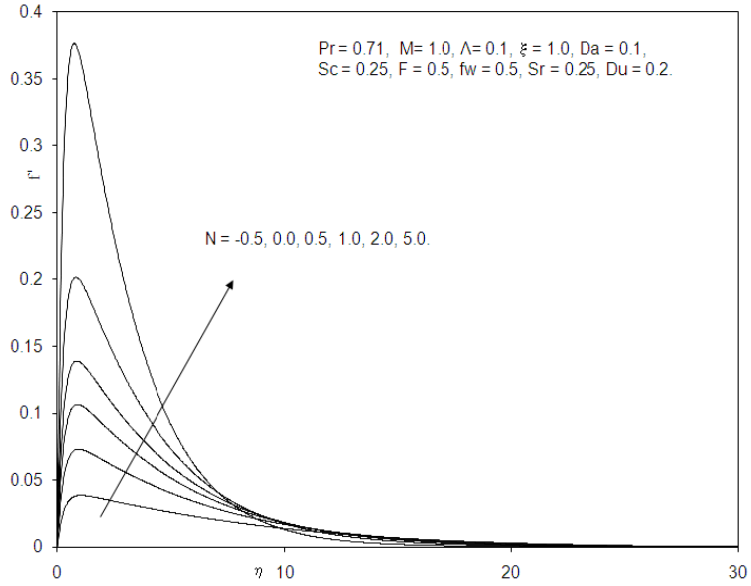

Fig.5a. Effect of N on the velocity profiles.

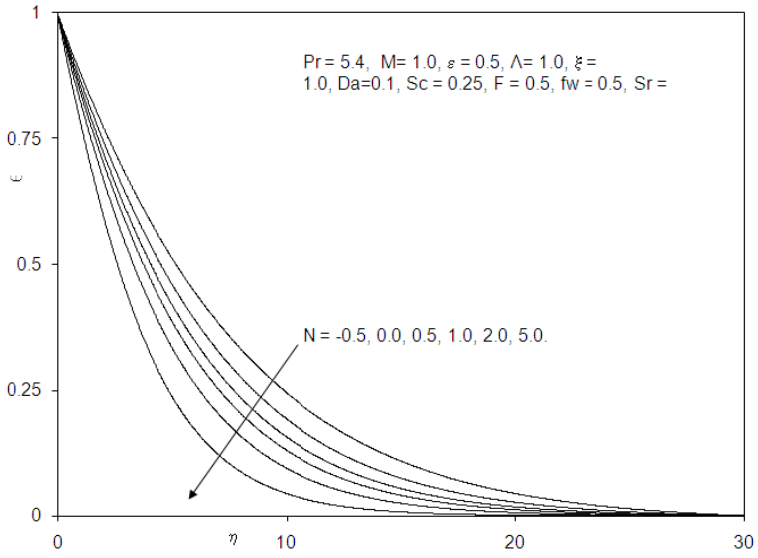

Fig.5b. Effect of N on the temperature profiles.

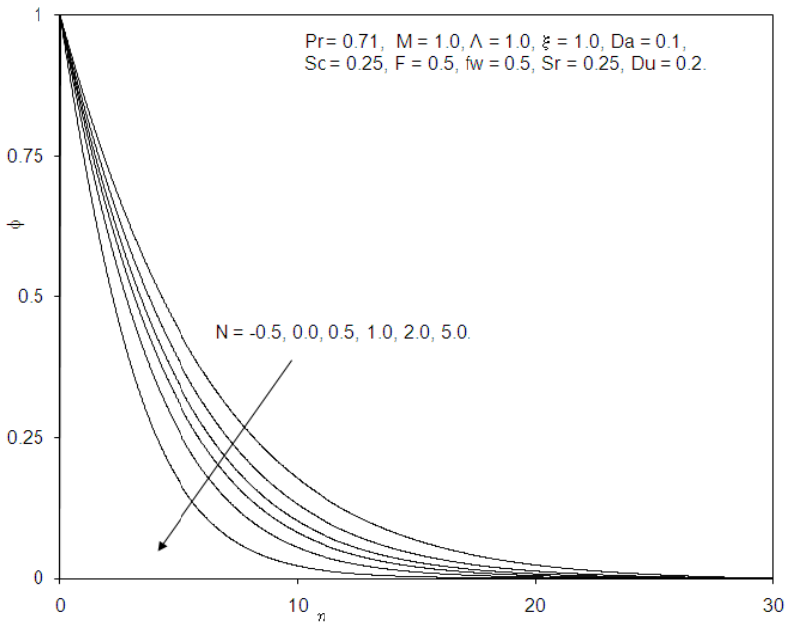

Fig.5c. Effect of *N* on the concentration profiles.

Figures 6a-c depict the velocity, temperature and species concentration distributions transverse to the cylinder wall for various stream wise coordinate values, ξ. Velocity is clearly decelerated with increasing migration from the leading edge, i.e., larger ξ values (Fig.6a) for some distance into the boundary layer, transverse to the wall (η ~ *8*). However, closer to the free stream, this effect is reversed and the flow is accelerated with increasing distance along the cylinder surface. Conversely, a very strong increase in temperature (θ) and concentration (ϕ), as shown in Figs 6b and 6c, occurs with increasing ξ values. Temperature and concentration are both minimized at the leading edge and maximized with the greatest distances along the cylinder surface from the leading edge.

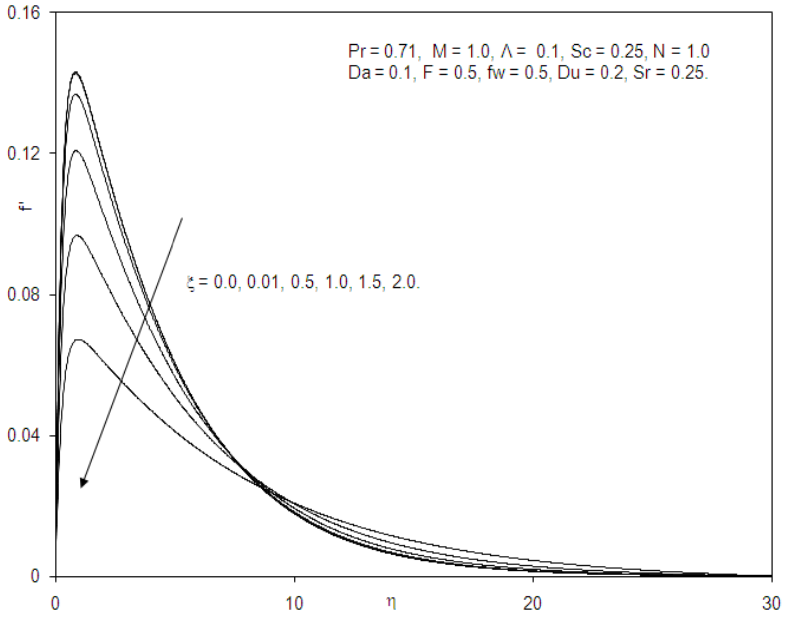

Fig.6a. The velocity profiles at various ξ.

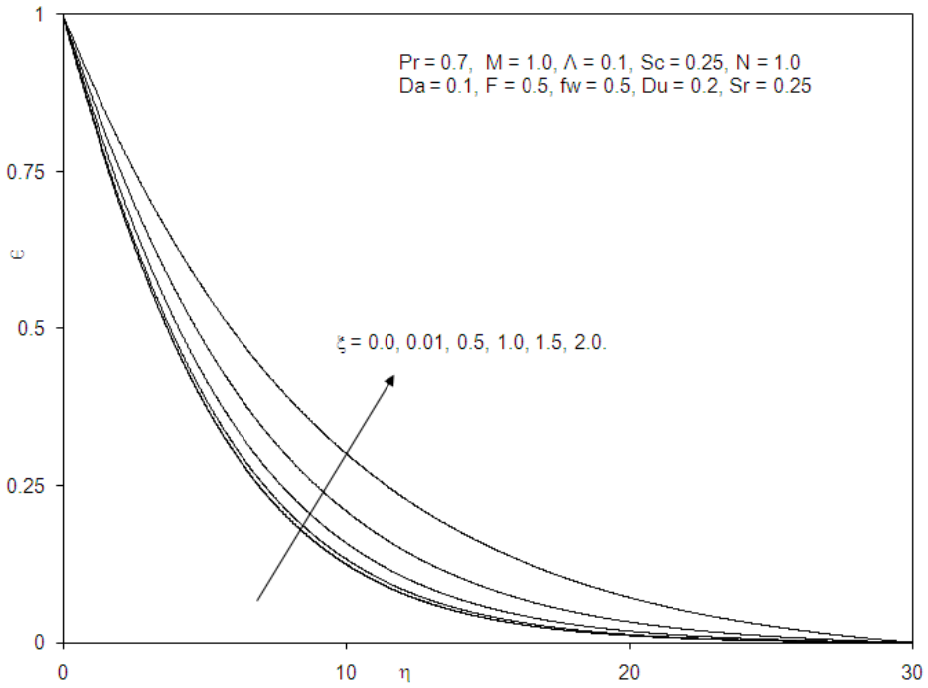

Fig.6b. The temperature profiles at various ξ.

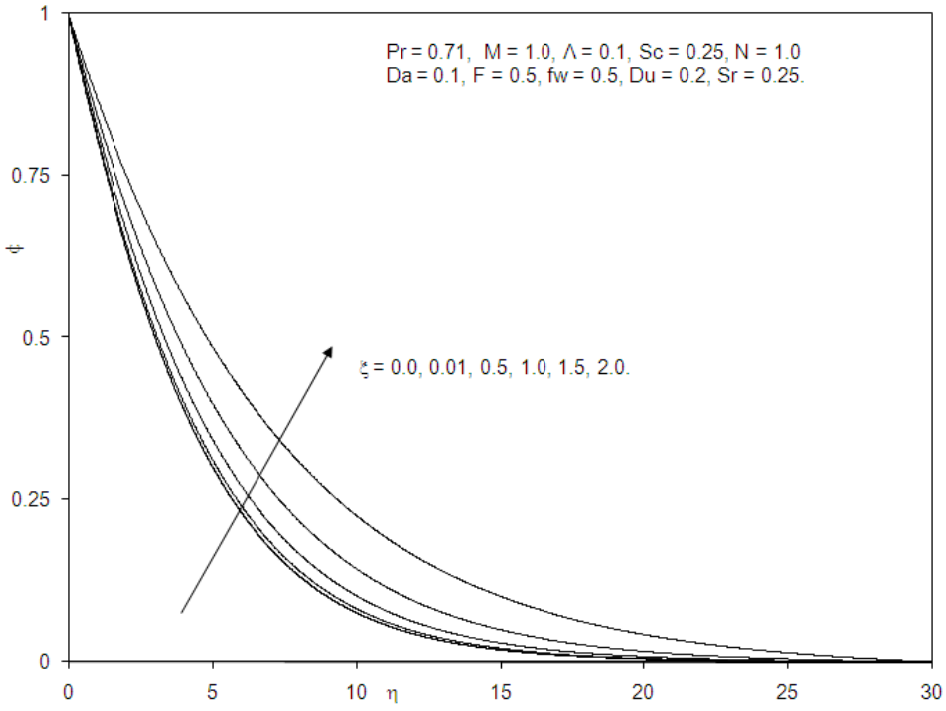

Fig.6c. The concentration profiles at various ξ.

Figures 7a-c illustrate the influence of wall transpiration on the velocity, temperature and species concentration functions with distance, η. With an increase in suction ($f_w>0$) the velocity is clearly decreased, i.e., the flow is decelerated. Increasing suction causes the boundary layer to adhere closer to the flow and

destroys momentum transfer; it is therefore an excellent control mechanism. Conversely, with increased blowing, i.e. injection of fluid via the cylinder surface into the porous medium regime, for which ($f_w<0$), the flow is accelerated i.e. velocities are increased. Temperature, θ and concentration ϕ, are also markedly enhanced with increased blowing at the cylinder wall and depressed with increased suction. The strong influence of wall transpiration on all the flow variables is impressively identified and again such a mechanism discussed earlier is greatly beneficial in allowing flow control and regulation of heat and mass transfer characteristics in, for example, materials processing from a cylindrical geometry.

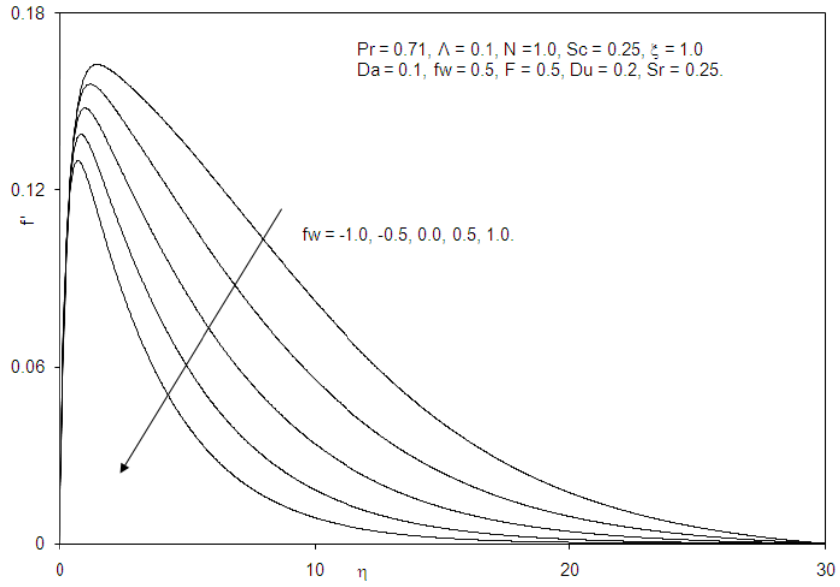

Fig.7a. Effect of *fw* on the velocity profiles.

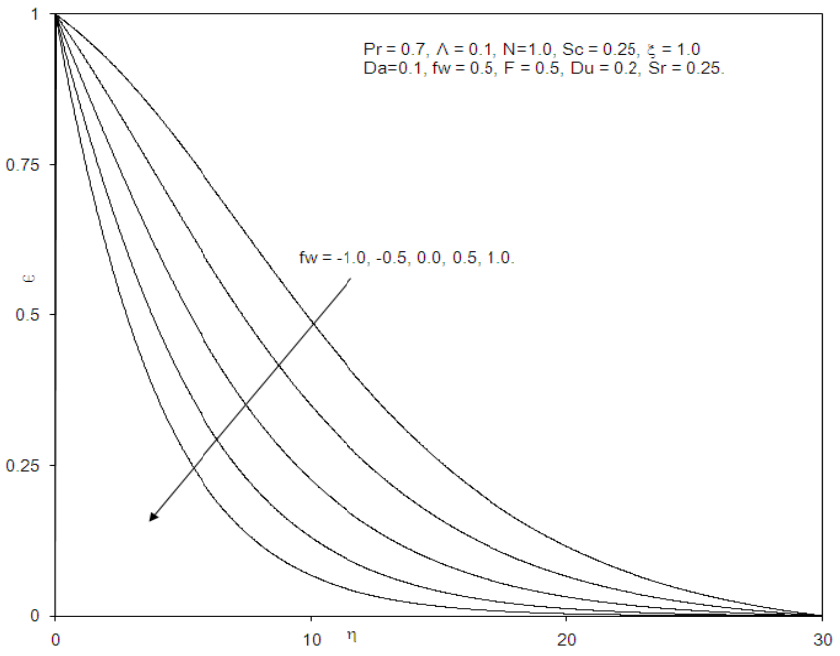

Fig.7b. Effect of *fw* on the temperature profiles.

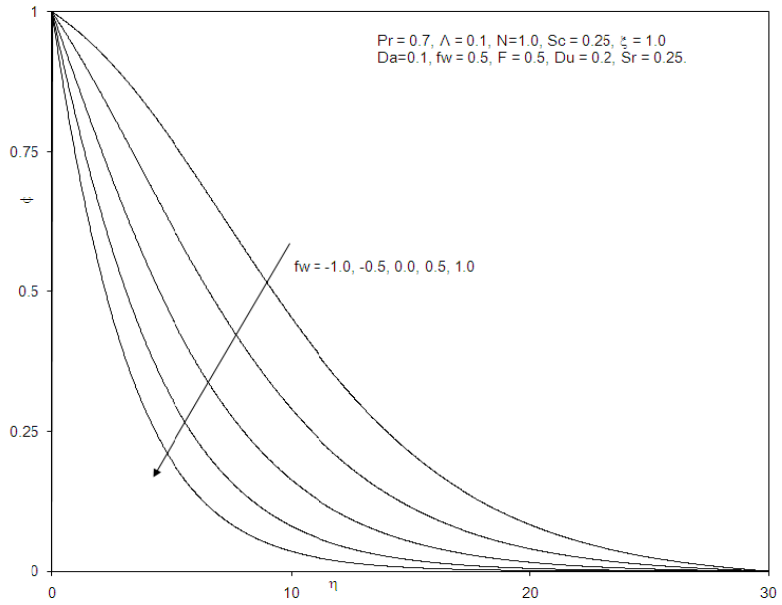

Fig.7c. Effect of *fw* on the concentration profiles.

The effect of the conduction radiation parameter, F on the cylinder surface shear stress, the local Nusselt number and local Sherwood number variations are presented in Figs 8a-c. With an increasing F, corresponding to progressively lower contributions of thermal radiation, the wall shear stress is consistently reduced, i.e., the flow is decelerated along the cylinder surface. With an increasing F, the local Nusselt number is considerably increased. Also, with an increasing F, local Sherwood number is decreased.

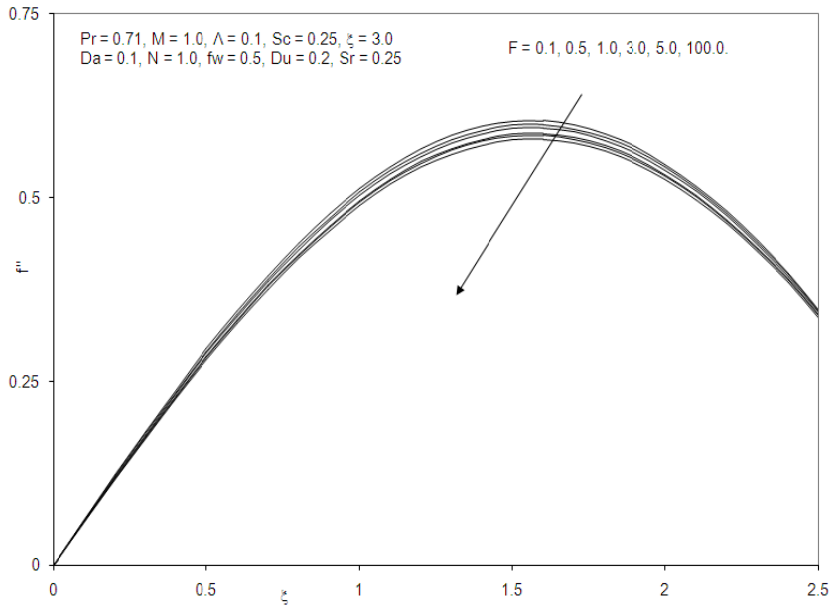

Fig.8a. Skin friction coefficient results for various values of F.

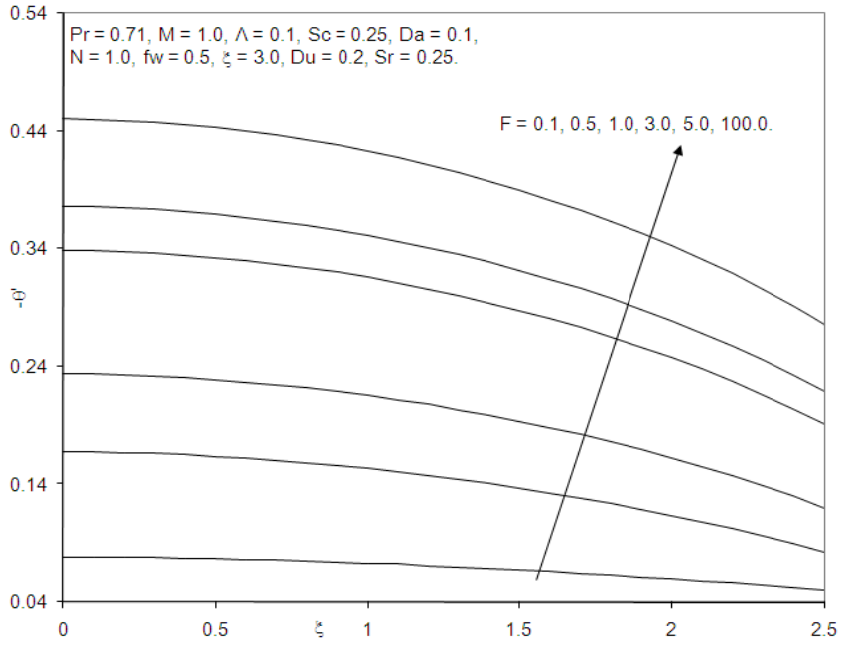

Fig.8b. Local Nusselt number results for various values of *F*.

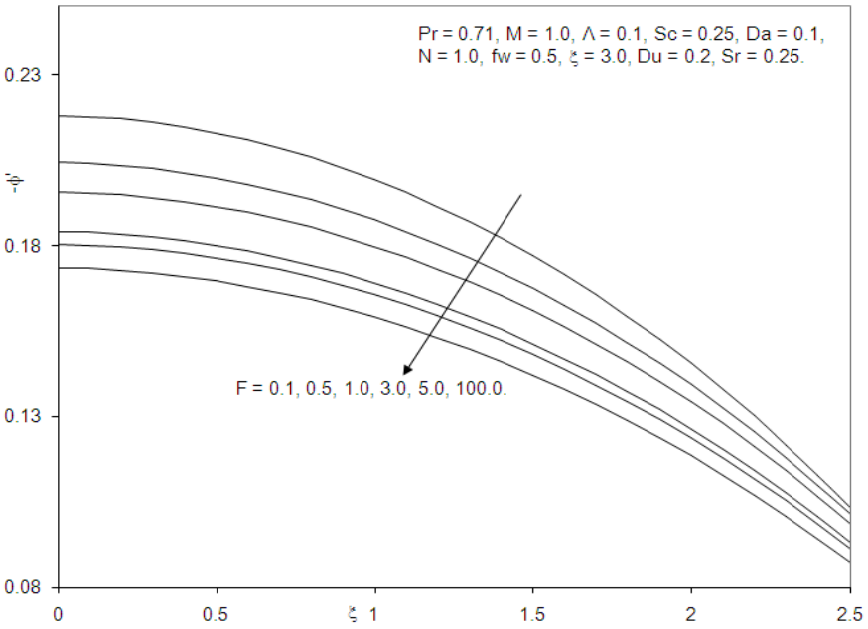

Fig.8c. Local Sherwood number results for various values of *F*.

Figure 9a shows the variation of the local Nusselt number, $-\theta'(\xi, 0)$ with the combined effects of the Soret and Dufour number. Increasing the Soret number (Sr) and simultaneously reducing the Dufour (Du) number greatly boost the local heat transfer rate at the cylinder surface. With increasing distance from the leading edge ($\xi = 0$), however, the profiles all decrease.

Figure 9b depicts the local Sherwood number distribution along the cylinder periphery (*x* coordinate) for various values of the Soret number (Sr) and Dufour number (Du). Sh is observed to strongly decrease with an increase in Sr and a simultaneous rise in Du. The largest decrease arises near the lower stagnation

point and the profiles tend to converge some distance thereafter, i.e., with progression along the cylinder periphery, while increasing Sr and decreasing Du still inhibit surface mass transfer rate, the effect is less pronounced.

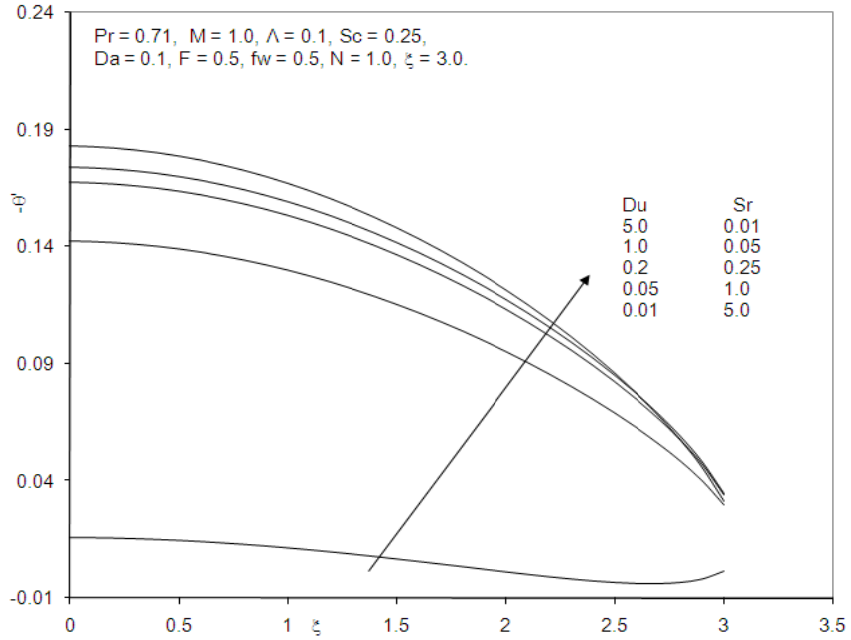

Fig.9a. Local Nusselt number results for various values of Sr and Du.

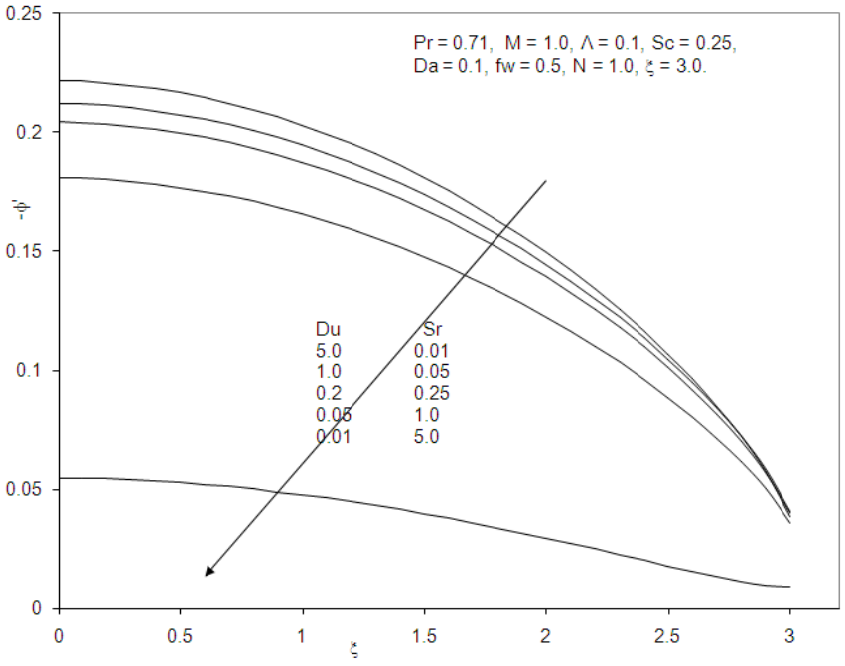

Fig.9b. Local Sherwood number results for various values of Sr and Du.

7. Conclusions

Hydromagnetic boundary layer heat and mass transfer flow from a horizontal cylinder immersed in a non-Darcy saturated porous medium is studied taking account of radiation and Soret/Dufour effects. A robust, validated implicit finite difference scheme has been employed. The results in summary have shown that,

i. Increasing the magnetic field parameter (M) reduces velocity but increases temperature and concentration.
ii. Increasing the Forchheimer inertial drag parameter (Λ) reduces velocity but elevates temperature and concentration.
iii. Increasing the radiation parameter (F) decreases velocity and temperature but increases concentration.
iv. Increasing the Soret number and simultaneously decreasing Dufour number enhance the local heat transfer rate (local Nusselt number) at the cylinder surface with the opposite effect sustained for the mass transfer rate (local Sherwood number).

Nomenclature

a − radius of the cylinder
B_0 − externally imposed radial magnetic field
C − concentration
Cf − skin friction coefficient
Da − Darcy parameter
Dm − mass diffusivity
F − radiation parameter
f − non-dimensional steam function
Gr − Grashof number
g − acceleration due to gravity
K − thermal diffusivity
k^* − mean absorption coefficient
M − magnetic parameter
N − buoyancy ratio parameter
Nu − local Nusselt number
Pr − Prandtl number
q_r − radiative heat flux
Sc − Schmidt number
Sh − local Sherwood number
T − temperature
u, v − non-dimensional velocity components along the x- and y- directions, respectively
x, y − non-dimensional Cartesian coordinates along the surface and its normal, respectively
α − thermal diffusivity
β, β^* − coefficients of thermal expansion and concentration expansion, respectively
Φ − azimuthal coordinate
ϕ − non-dimensional concentration
Γ − the Forchheimer inertial drag coefficient
η − dimensionless radial coordinate
μ − dynamic viscosity
ν − kinematic viscosity
θ − non-dimensional temperature
ρ − density
σ − electrical conductivity

σ^* − the Stefan-Boltzmann constant
ξ − dimensionless tangential coordinate
ψ − dimensionless stream function

Subscripts

w − conditions on the wall
∞ − free stream conditions

Superscripts

‘− differentiation with respect to η

References

[1] Escobar F.H. and Civan F. (1996): *Quadrature solution for foam flow in porous media*. − J. Petroleum Science and Engineering, vol.15, pp.379-387.

[2] Ng E.Y.K., Ghista D.N. and Jegathese R.C. (2005): *Perfusion studies of steady flow in in poroelastic myocardium tissue*. Computer Methods in Biomechanics and Biomedical Engineering, vol.8, pp.349-357.

[3] Nicholson C. (2001): *Diffusion and related transport mechanism in brain tissue*. − Rep. Prog. Phys., vol.64, pp.815-884.

[4] Jinliang Wang Catton I. (2001): *Bi porous heat pipes for high power electronic device cooling*. − Semiconductor Thermal Measurement and Management, 2001. Seventeenth Annual IEEE Symposium, pp.211 – 218, San Jose, California, USA.

[5] Douglas J. Jr, Pereira F. and Li-Ming Yeh (2000): *A locally conservative Eulerian–Lagrangian numerical method and its application to nonlinear transport in porous media*. − Computational Geosciences, vol.4, pp.1-40.

[6] Cheng H-P. and Yeh G-T. (1998): *Development and demonstrative application of a 3-D numerical model of subsurface flow, heat transfer, and reactive chemical transport: 3DHYDROGEOCHEM*. − J. Contaminant Hydrology, vol.34, pp.47-83.

[7] Laschet G., Sauerhering J., Reutter O., Fend T. and Scheele J. (2009): *Effective permeability and thermal conductivity of open-cell metallic foams via homogenization on a microstructure model*. − Computational Materials Science, vol.45, pp.597-603.

[8] Becker M., Fend Th., Hoffschmidt B., Pitz-Paal R., Reutter O., Stamatov V., Steven M. and Trimis D. (2006): *Theoretical and numerical investigation of flow stability in porous materials applied as volumetric solar receivers*. − Solar Energy, vol.80, pp.1241-1248.

[9] Roblee L.H.S., Baird R.M. and Tiernery J.W. (1958): *Radial porosity variation in packed beds*. − AIChemE J., vol.8, pp.359-61.

[10] Vafai K. (1984): *Convective flow and heat transfer in variable-porosity media*. − J. Fluid Mechanics, vol.147, pp.233-259.

[11] Zueco J., Anwar Bég O. and Takhar H.S. (2009): *Network numerical analysis of magneto-micropolar convection through a vertical circular non-Darcian porous medium conduit*. − Computational Materials Science, vol.46, pp.1028-1037.

[12] Makinde O.D., Anwar Bég O. and Takhar H.S. (2009): *Magnetohydrodynamic viscous flow in a rotating porous medium cylindrical annulus with an applied radial magnetic field*. − Int. J. Applied Mathematics and Mechanics, vol.5, No.6, pp.68-81.

[13] Damseh R.A., Tahat M.S. and Benim A.C. (2009): *Nonsimilar solutions of magnetohydrodynamic and thermophoresis particle deposition on mixed convection problem in porous media along a vertical surface with variable wall temperature*. − Progress in Computational Fluid Dynamics: An International Journal, vol.9, pp.58-65.

[14] Minkowycz W.J. and Cheng P. (1976): *Free convection about a vertical cylinder embedded in a porous medium*. − Int. J. Heat Mass Transfer, vol.19, pp.508-513.

[15] Hamzeh Alkasasbeh T., Mohd Zuki Salleh, Roslinda Nazar and Ioan Pop (2014): *Numerical solutions of radiation effect on magnetohydrodynamic free convection boundary layer flow about a solid sphere with Newtonian heating*. − Applied Mathematical Sciences, vol.8, No.140, pp.6989-7000.

[16] Kumari M and Gorla R.S.R. (2015): *MHD boundary layer flow of a non-Newtonian nanofluid past a wedge*. − Journal of Nanofluids, vol.4, No. 1, March, pp.73-81(9).

[17] Takhar H.S., Bég O.A. and Kumari M. (1998): *Computational analysis of coupled radiation-convection dissipative non-gray gas flow in a non-Darcy porous medium using the Keller-Box implicit difference scheme*. − Int. J. Energy Research, vol.22, pp.141-159.

[18] Takhar H.S., Bég O.A., Chamkha A.J., Filip D. and Pop I. (2003): *Mixed radiation-convection boundary layer flow of an optically dense fluid along a vertical flat plate in a non-Darcy porous medium*. − Int. J. Applied Mechanics Engineering, vol.8, pp.483-496.

[19] Hossain Md. A. and Pop I. (2001): *Studied radiation effects on free convection over a flat plate embedded in a porous medium with high-porosity*. − Int. J. Therm. Sci., vol.40, pp.289-295.

[20] Dulal Pal and Sewli Chatterjee (2013*): Soret and Dufour effects on MHD convective heat and mass transfer of a power-law fluid over an inclined plate with variable thermal conductivity in a porous medium*. − Applied Mathematics and Computation, vol.219, No.14, pp.7556–7574.

[21] Abreu C.R.A., Alfradique M.F. and Silva Telles A. (2006): *Boundary layer flows with Dufour and Soret effects: I: Forced and natural convection*.− Chemical Engineering Science, vol.61, No.13, pp.4282-4289.

[22] Bég O.A., Tasveer A., BégA.Y. Bakier and Prasad V. (2009): *Chemically-reacting mixed convective heat and mass transfer along inclined and vertical plates with Soret and Dufour effects: Numerical solutions*.− Int. J. Applied Mathematics and Mechanics, vol.5, No.2, pp.39-57.

[23] Bhargava R., Sharmaand R. and Bég O.A. (2009): *Oscillatory chemically-reacting MHD free convection heat and mass transfer in a porous medium with Soret and Dufour effects: finite element modeling*.− Int. J. Applied Mathematics and Mechanics, vol.5, No.6, pp.15-37.

[24] Seddeek M.A. (2004): *Thermal-diffusion and diffusion-thermo effects on mixed free-forced convective flow and mass transfer over accelerating surface with a heat source in the presence of suction and blowing in the case of variable viscosity*. − Acta Mech., vol.172, pp.83-94.

[25] El-Kabeir S.M.M and Chamkha Ali J. (2013): *Heat and mass transfer by mixed convection from a vertical slender cylinder with chemical reaction and Soret and Dufour effects*. − Heat Transfer-Asian Research, vol.42, No.7, pp.618-629.

[26] Bhattacharyya K., Layek G.C. and Seth G.S. (2014): *Soret and Dufour effects on convective heat and mass transfer in stagnation-point flow towards a shrinking surface*.− Phys. Scr. vol.89, No.9, 095203.

[27] Yih K.A. (2000): *Effect of uniform blowing/suction on MHD-natural convection over a horizontal cylinder: UWT or UHF*. − Acta Mechanica, vol.44, pp.17-27.

[28] Modest M.F. (1993): *Radiation Heat Transfer*. − New York: MacGraw-Hill.

[29] Raptis P. and Perdikis C. (2004): *Unsteady flow through a highly porous medium in the presence of radiation*. − Transport Porous Medium J., Vol. 57(2), pp. 171-179.

[30] Cebeci T. and Bradshaw P. (1984): *Physical and Computational Aspects of Convective Heat Transfer*.− New York: Springer.

[31] Rama Subba Reddy Gorla and Buddakkagari Vasu (2016): *Unsteady convective heat transfer to a stretching surface in a non-Newtonian nanofluid*. −Journal of Nanofluids, vol.5, No.4, pp.581-594.

[32] Merkin J.H. (1977): *Free convection boundary layers on cylinders of elliptic cross section*. − J. Heat Transfer, vol.99, pp.453-457.

Received: February 9, 2018

Revised: September 2, 2019